

This is a repository copy of *Initial operation of the recoil mass spectrometer EMMA at the ISAC-II facility of TRIUMF*.

White Rose Research Online URL for this paper:

<https://eprints.whiterose.ac.uk/147401/>

Version: Accepted Version

Article:

Davids, B., Williams, M., Esker, N. E. et al. (8 more authors) (2019) Initial operation of the recoil mass spectrometer EMMA at the ISAC-II facility of TRIUMF. Nuclear Instruments and Methods in Physics Research, Section A: Accelerators, Spectrometers, Detectors and Associated Equipment. pp. 191-195. ISSN 0168-9002

<https://doi.org/10.1016/j.nima.2019.03.070>

Reuse

This article is distributed under the terms of the Creative Commons Attribution-NonCommercial-NoDerivs (CC BY-NC-ND) licence. This licence only allows you to download this work and share it with others as long as you credit the authors, but you can't change the article in any way or use it commercially. More information and the full terms of the licence here: <https://creativecommons.org/licenses/>

Takedown

If you consider content in White Rose Research Online to be in breach of UK law, please notify us by emailing eprints@whiterose.ac.uk including the URL of the record and the reason for the withdrawal request.

Initial Operation of the Recoil Mass Spectrometer EMMA at the ISAC-II Facility of TRIUMF

B. Davids^{a,b}, M. Williams^{a,c}, N.E. Esker^a, M. Alcorta^a, D. Connolly^a,
B.R. Fulton^c, K. Hudson^{a,b}, N. Khan^a, O.S. Kirsebom^a, J. Lighthall^a,
P. Machule^a

^a*TRIUMF, 4004 Wesbrook Mall, Vancouver, BC, V6T 2A3, Canada*

^b*Department of Physics, Simon Fraser University, 8888 University Drive, Burnaby, BC,
V5A 1S6, Canada*

^c*Department of Physics, University of York, Heslington, York, YO10 5DD,
United Kingdom*

Abstract

The Electromagnetic Mass Analyser (EMMA) is a new vacuum-mode recoil mass spectrometer currently undergoing the final stages of commissioning at the ISAC-II facility of TRIUMF. EMMA employs a symmetric configuration of electrostatic and magnetic deflectors to separate the products of nuclear reactions from the beam, focus them in both energy and angle, and disperse them in a focal plane according to their mass/charge (m/q) ratios. The spectrometer was designed to accommodate the γ -ray detector array TIGRESS around the target position in order to provide spectroscopic information from electromagnetic transitions. EMMA is intended to be used in the measurement of fusion evaporation, radiative capture, and transfer reactions for the study of nuclear structure and astrophysics. Its complement of focal plane detectors facilitates the identification of recoiling nuclei and subsequent recoil decay spectroscopy. Here we describe the facility and report on commissioning efforts.

Keywords: Recoil mass spectrometer, electromagnetic separator, recoil separator

1. Introduction

The Electromagnetic Mass Analyser (EMMA) [1] has been installed at the ISAC-II facility of TRIUMF [2]. EMMA is a vacuum-mode recoil mass spectrometer designed to separate the recoils of nuclear reactions from the primary beam, focus them in energy and angle, and disperse them in a focal plane according to their mass/charge (m/q) ratios. The spectrometer is fixed at 0° with respect to the beam axis and is mounted on a common support platform with 1.5 m of longitudinal travel, allowing for the positioning of various detector arrays at the target position, including the γ -ray spectrometer TIGRESS [3] and the Si charged particle detector array SHARC [4]. As depicted in Figure 1, EMMA uses a symmetric configuration of two electrostatic deflectors and a dipole magnet to focus reaction products in kinetic energy/charge (E/q). Angular focusing is achieved via quadrupole doublets at the entrance and exit of the spectrometer, the latter of which enables variable m/q dispersion. A photograph of the spectrometer taken in December 2016 is shown in Figure 2.

2. Ion Optics

The ion optical design of EMMA is similar to those of the Rochester RMS [5, 6], CAMEL at Legnaro [7, 8, 9], the Oak Ridge RMS [10, 11, 12], HIRA at IUAC [13, 14], the JAERI RMS [15, 16, 17], and the Argonne Fragment Mass Analyzer (FMA) [18, 19, 20]; it was optimized to provide large

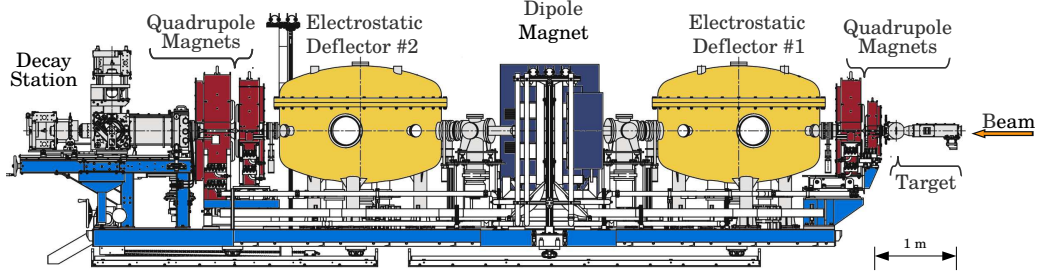


Figure 1: Schematic side view of EMMA, showing the target chamber, quadrupole and dipole magnets, electrostatic deflectors, and focal plane detector chamber surrounded by γ -ray detectors. The spectrometer is mounted on a platform capable of 1.5 m of travel along the beam direction.

22 acceptance without unduly compromising the resolving power necessary to
 23 study transfer reactions in inverse kinematics as well as fusion evaporation
 24 reactions. To that end, EMMA features electrodes with larger bending radii
 25 and a shorter first quadrupole magnet than the FMA. The EMMA electrodes
 26 have the same bending radii as those of HIRA and are smaller than those of
 27 the Oak Ridge RMS. For ions of a given electrostatic rigidity, larger electrode
 28 bending radii allow operation at lower voltages. The ion optics code GIOS
 29 [21] was used to design the spectrometer, both initially and again after the
 30 electromagnetic elements were fabricated, to take account of the differences
 31 between their specified and as-built properties. The standard achromatic ion
 32 optical tune has a vertical crossover in the centre of the dipole magnet and
 33 m/q dispersion ($x|\delta_m \equiv \frac{\partial x}{\partial \delta_m}$) of 10 mm/%. Here, x is the horizontal displace-
 34 ment with respect to the optic axis in the focal plane and $\delta_m \equiv \frac{m/q - m_0/q_0}{m_0/q_0}$ is
 35 the fractional m/q deviation with respect to that of the central reference tra-
 36 jectory, m_0/q_0 . Two quadrupole doublets permit variable angular focussing

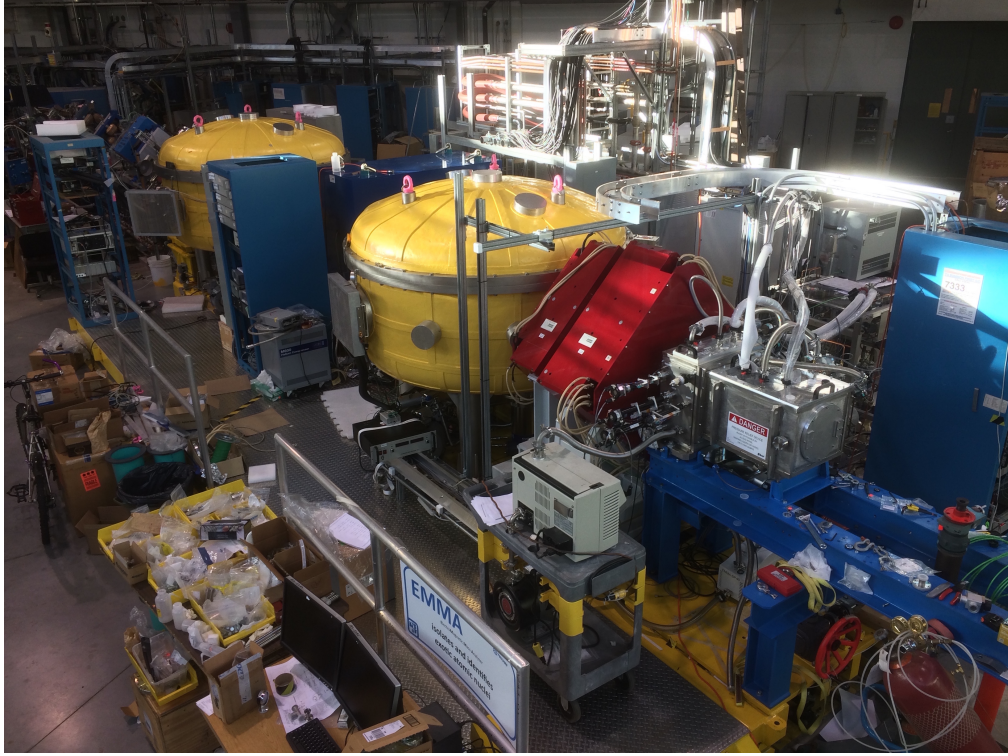


Figure 2: Photograph of EMMA taken in December 2016.

37 modes; by changing the fields in the second doublet, the m/q dispersion can
 38 be varied continuously between 0 and 20 mm/%.

39 To first order, given the bending angles and radii of curvature of the
 40 electrostatic deflectors and the dipole magnet as well as the edge angles
 41 of the latter, EMMA achieves energy focussing on account of the 1225 mm
 42 separation between the effective field boundaries of the dipole magnet and the
 43 electrostatic deflectors on either side of it. Mathematically this is expressed
 44 as $(x|\delta_E) \equiv \frac{\partial x}{\partial \delta_E} = 0$ and $(a|\delta_E) = 0$. The fractional kinetic energy/charge
 45 deviation with respect to that of the central reference trajectory, E_0/q_0 , is
 46 defined as $\delta_E = \frac{E/q - E_0/q_0}{E_0/q_0}$ and $a \equiv p_x/p_0 \approx \theta$, the horizontal angle with

Table 1: As-Built EMMA Dimensions and Maximum Fields

Length from target to focal plane (m)	9.143		
Dipoles	MD	ED1, ED2	
Radius of curvature (m)	1.0	5.0	
Deflection angle ($^{\circ}$)	40.11	20.05	
Entrance and exit inclination angles ($^{\circ}$)	7.93, 8.67	—	
Effective field boundary radii (m)	3.472	—	
Pole gap (cm)	12	12.5	
Maximum field	1.0 T	40 kV/cm	
Maximum rigidity	1.0 T m	20 MV	
Magnetic lenses	Q1	Q2, Q3	Q4
Bore diameter (cm)	7	15	20
Effective length (cm)	14.0	30.0	40.2
Maximum pole tip field (T)	1.21	0.84	0.80
Maximum field gradient (T/m)	35	12	8.1

47 respect to the optic axis. Here p_x is the horizontal projection of the ion
 48 momentum and p_0 is the total momentum of the reference trajectory. In
 49 the horizontal direction the angular acceptance is defined by the gap of the
 50 first electrostatic deflector and in the vertical direction it is defined by the
 51 vacuum chamber of the first quadrupole magnet. The standard distance from
 52 the target to the effective field boundary of the first quadrupole is 25 cm and
 53 the focal plane position is variable but in the standard tune lies 32 cm from
 54 the effective field boundary of the fourth quadrupole.

55 **3. Electromagnetic Elements**

56 The quadrupole and dipole magnets, their power supplies, and most of the
57 components of the electrostatic deflectors were fabricated by Bruker BioSpin,
58 S. A. S. of Karlsruhe, Germany, whereas the other custom hardware was
59 constructed at TRIUMF, including the high voltage power supplies for the
60 deflectors. Each of the magnetic elements was mapped by the manufacturer
61 with a Hall effect magnetometer prior to shipment. All of the fringing fields
62 were mapped along with the central fields. The as-built properties of the
63 electromagnetic elements are given in Table 1.

64 *3.1. Quadrupole Lenses*

65 EMMA’s first quadrupole lens (Q1) was designed to have high pole tip
66 fields and a short effective length to minimize chromatic aberrations. Its
67 cantilevered support was built so as not to interfere with the placement of
68 12 of the 16 TIGRESS high purity germanium (HPGe) detectors around the
69 target position while simultaneously keeping the target to Q1 effective field
70 boundary separation small, thereby maximizing angular acceptance. The
71 quadrupoles are arranged in two doublets, Q1-Q2 and Q3-Q4. Both Q2 and
72 Q3 were fabricated according to the same design, while Q1 is smaller; Q4
73 is larger in order to transmit m/q -dispersed ions. Field clamps installed on
74 the upstream and downstream sides of each doublet limit the extent of the
75 fringing fields, which is particularly important given the presence of HPGe
76 detector photomultiplier tubes nearby at the target and focal plane positions.
77 At the factory, the higher multipole components, effective field boundaries,
78 and deviations between the mechanical and magnetic axes were measured

79 with the field clamps in place and found to meet our specifications.

80 A transverse Hall probe inserted just below the bore of each quadrupole
81 is used as a reference to set and monitor its field. The Hall effect mag-
82 netometers used in all the magnets are model FM-3000-BB-10 Teslameters
83 produced by Projekt Elektronik Mess- und Regelungstechnik GMBH. The
84 field gradient was measured as a function of the reference Hall probe voltage.
85 For each quadrupole, a cylindrical holder with multiple Hall probe positions
86 was precisely machined and aligned, via a laser tracker, to make these mea-
87 surements. Corrections due to the < 0.1 mm offset between the mechanical
88 and magnetic axes obtained from the factory field map were neglected. This
89 method produced a calibration that allows the field gradient to be inferred
90 from the reference probe voltage to a precision of 0.1%. Accurate calibration
91 of the Hall effect magnetometers was confirmed by comparing with an NMR
92 magnetometer using a uniform dipole reference field.

93 *3.2. Dipole Magnet*

94 The dipole magnet is a 40° homogeneous field magnetic sector that was
95 specified to have effective field boundaries (EFBs) inclined by 8.3° with re-
96 spect to normal incidence. In order to reduce the horizontal focussing of
97 the sector and increase its vertical focussing, these inclinations are such that
98 ions following trajectories with large bending radii pass through less field and
99 those on small-radius trajectories pass through more field than they would
100 in the case of normal incidence. The poles of the magnet were designed in
101 a three-piece arrangement with small pole edge inserts on either side of a
102 large central piece. These pole edge inserts were machined and re-machined
103 until the measured inclinations of the entrance and exit EFBs were 7.93°

104 and 8.67° , respectively. The average of the two is 8.3° ; the effect of these
 105 distinct entrance and exit angles on the overall ion optical performance of
 106 the spectrometer was studied using GIOS and found to be compatible with
 107 the design requirements after a slight (< 1 mm) adjustment to the separa-
 108 tions between the effective field boundaries of the magnet and the EDs.
 109 Each effective field boundary is curved with a radius of 3.47 m to provide a
 110 second order correction designed to minimize the $(x|\delta_E^2)$ term. An 8 mm ver-
 111 tical gap between the bottom pole and the vacuum chamber was preserved
 112 to allow the placement of thin correction coils on the pole face should they
 113 be deemed necessary. A decision to fabricate and install such coils would
 114 be made only after a detailed study of ion optical aberrations, which is not
 115 currently planned. The field is measured by a Hall probe fixed to the bottom
 116 pole piece at a location well within the uniform field region.

117 The dipole magnet vacuum chamber has rectangular entrance and exit
 118 apertures that measure 205 mm horizontally and 92 mm vertically. In the
 119 central region the chamber expands to a maximum horizontal extent of 491
 120 mm. Two straight-through ports aligned with the incoming and outgoing
 121 beam axes proved useful when aligning the slit systems located at the en-
 122 trance and exit of the chamber. Sheets of aluminum honeycomb cores made
 123 by Plascore line the vertical walls and bottom surface of the vacuum chamber
 124 to minimize scattering of ions on grazing trajectories. The honeycomb cells
 125 are 6.35 mm in diameter and the sheets are 3.2 mm thick.

126 *3.3. Electrostatic Deflectors*

127 Each of the two electrostatic deflectors (EDs) includes a pair of polished
 128 solid titanium electrodes backed by an array of Ti ribs intended to provide

129 structural stability. The ribs and the 25 mm thick electrode of each cathode
130 were machined from a single piece of Ti, as were the 20 mm thick, rib-backed
131 anodes, which were bolstered from behind with an additional ribbed piece
132 of Ti. Each of the four electrodes is supported by four cylindrical ceramic
133 insulators. The insulators were brazed into Ti feet that attach to adjustable,
134 polished Al mounting blocks connected to an Al support frame that rests
135 in a stainless steel vacuum vessel. The vacuum-insulator-conductor triple
136 points are shielded by Al corona rings and all sharp corners and edges are
137 concealed behind polished electrostatic shields fashioned from Al. Figure 3
138 shows the interior of the ED2 vacuum tank. All the components subject to
139 high electric fields were polished extensively using a combination of fine grit
140 sandpaper and a succession of five varying grades of diamond pastes from
141 9 μm down to 0.25 μm grit sizes. For the rounded electrode surfaces that
142 sustain the highest fields, an additional phase of polishing with a colloidal
143 silica suspension was employed.

144 The electrode support structures were assembled in a clean room to min-
145 imize dust deposition on the surfaces. Alignment of the electrode pairs was
146 done to a precision of 0.1 mm inside the clean room using a FARO coordinate
147 measuring machine with an articulating arm and a Leica laser tracker. Dur-
148 ing the alignment procedure a significant discrepancy was discovered between
149 the measured and specified radii of curvature of the anodes; they are listed
150 for comparison in Table 2. The electrodes were positioned such that the gap
151 between them is 125 mm in the centre, which results in a reduction of the gap
152 at the electrode edges compared with the design due to the smaller radii of
153 curvature of the anodes. This manufacturing defect means that the electric

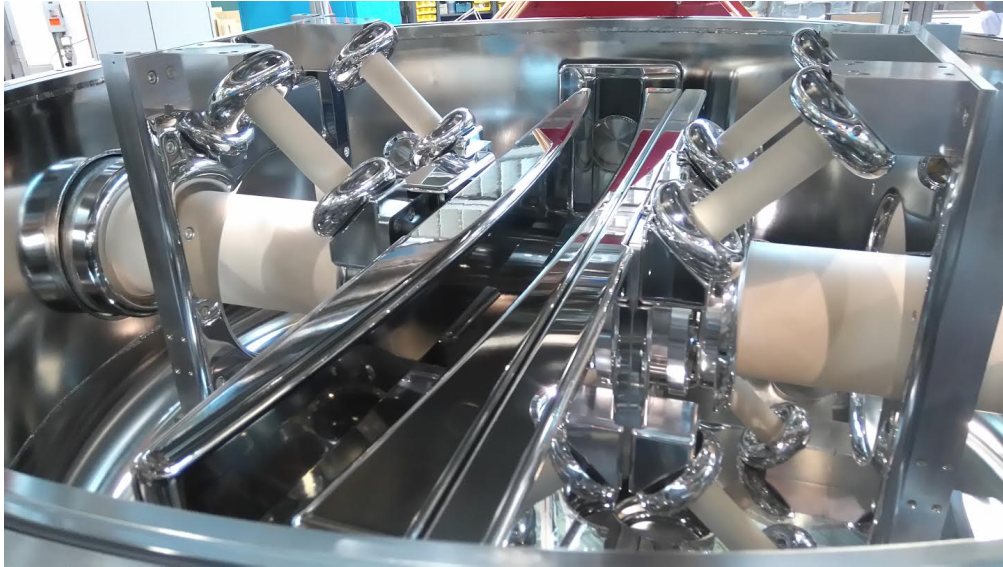


Figure 3: Photograph of the interior of the 2nd electrostatic deflector vacuum vessel.

154 fields in the gap are not as homogeneous as specified and that unanticipated
 155 second- and higher-order ion optical aberrations are present in the system; it
 156 also implies that the first order energy dispersion ($x|\delta_E$) is not quite as small
 157 as planned. These flaws were highly impractical to correct, as the polished,
 158 cleaned, and aligned electrodes would have had to be removed, re-machined,
 159 and re-polished.

160 High voltage is provided to the electrodes via internal, 40 stage full-
 161 wave Cockcroft-Walton DC multipliers built at TRIUMF. The multipliers are
 162 driven by external 1 kW Glassman High Voltage Inc. PG010K100JD2DRV
 163 DC supplies that allow for constant voltage or constant current operation.

Table 2: EMMA Electrode Radii of Curvature in mm

Electrode	ED1	ED2	Specification
Anode	5007.3(55)	4977.1(55)	5062.5
Cathode	4953.3(55)	4952.0(55)	4937.5

Each multiplier has been tested without a load to a maximum potential difference of at least 325 kV. To prevent breakdown the multipliers are housed within re-entrant ceramic vessels pressurized with 3 bar of electrically insulating SF₆ gas. As bias is applied during conditioning, steady state load currents can reach as much as 35 μ A, leading to the emission of X-rays. For shielding purposes, the entire surface of the stainless steel dipole vacuum vessels are covered with 6.35 mm thick lead sheets cut and pounded into various shapes that were affixed using epoxy. All the ports and windows are covered with caps containing the same thickness of Pb. Thus far, the first and second electrostatic deflectors have been conditioned to maximum stable potential differences of 340 kV and 440 kV, respectively. We plan to condition them further to a potential difference of 500 kV.

Each electrostatic deflector vacuum tank is pumped by an Agilent TV1001 1000 L/s turbomolecular pump, an Oxford Instruments CryoPlex 8 1500 L/s cryopump, and a Gamma Vacuum TiTan 600L 500 L/s ion pump. The ion pumps run on a diesel-generator-backed uninterruptible electric power circuit in order to ensure high vacuum continuously through electric power bumps and failures. Pressures in the mid 10^{-9} Torr range are typically observed with only two pumps running in each isolated vessel.

183 4. Experimental Apparatus

184 Two 10" OD ConFlat vacuum crosses mounted symmetrically between
185 the electrostatic deflectors and the dipole magnet house horizontal slit sys-
186 tems that can block ions on unwanted trajectories. The two 1.6 mm thick
187 stainless steel plates that make up each slit system can be driven indepen-
188 dently to create an opening from 0-180 mm wide. The opening need not be
189 centred on the optic axis. One cross has a 1500 L/s cryopump and the other
190 has a 1000 L/s turbomolecular pump. When either of these pumps is used
191 to evacuate the isolated MD vacuum chamber section a pressure in the low
192 10^{-9} Torr range is typically observed.

193 Several experimental systems have been designed and installed at EMMA
194 while others are still under construction. These include target and focal plane
195 detector systems and their associated chambers and accessories. Notably,
196 some are being developed with off-site collaborators, such as those at the
197 University of York in the UK.

198 A 20 cm diameter spherical target chamber couples to the vacuum cham-
199 ber of the first quadrupole magnet. The chamber is designed to accommodate
200 12 TIGRESS detectors in a closely packed configuration. It contains a ro-
201 tary target mechanism that allows for the manual positioning of up to three
202 target foil positions into the beam path. The target chamber also houses an
203 integral, suppressed Faraday cup on a separate rotary actuator; a Ta aper-
204 ture plate at its entrance lies in the same plane as the target foils. The Ta
205 plate has a 1 mm diameter aperture through which the beam is tuned by
206 maximizing the current on the Faraday cup while minimizing that on the
207 aperture plate.

208 The target chamber has provisions for mounting two 150 mm² silicon
 209 surface barrier detectors centred at 20° angles with respect to the beam
 210 axis downstream of the target. They are used to monitor the beam flux
 211 and target condition via elastic scattering and are primarily intended for
 212 the normalization of reaction cross section measurements. Additionally, a
 213 highly-segmented, annular silicon detector can be mounted 33 mm upstream
 214 or downstream of the target position to detect light charged particles. A thin
 215 C foil can be positioned 116 mm downstream of the target position in order
 216 to restore the charge state distributions of transmitted ions to equilibrium
 217 through charge-changing collisions following possible internal conversion de-
 218 cays. Similarly, an energy degrader foil can be mounted 68 mm downstream
 219 of the target. To exclude ions on trajectories outside of the angular ac-
 220 ceptance of the spectrometer, a circular aperture at the exit of the target
 221 chamber defines a cone of half-angle 4.2° and a solid angle of 17 msr; an ad-
 222 ditional, optional $\pm 2^\circ$ aperture can be used to restrict the horizontal angular
 223 acceptance when high m/q resolving power is required, as described in Ref.
 224 [1].

225 A separate target chamber designed to accommodate highly-segmented
 226 rectangular and annular silicon detectors as well as 12 TIGRESS detectors,
 227 dubbed SHARC-II, has been designed at the University of York and is in the
 228 final stages of fabrication. It can be positioned so that the target is separated
 229 from the Q1 effective field boundary by the standard 25 cm.

230 The focal plane station has a modular design in which detectors may
 231 be inserted and removed easily according to the experimental requirements.
 232 A position-sensitive parallel grid avalanche counter (PGAC) and an energy-

233 sensitive ionization chamber (IC) make up the standard complement of focal
 234 plane detectors. They are mounted in separate vacuum chambers that can be
 235 joined together, allowing for the use of the PGAC without the IC if energy
 236 loss signals are not required. In the current configuration, the use of the
 237 PGAC is mandatory while the IC is optional. A 3000 mm² ion-implanted Si
 238 detector can be mounted directly behind the PGAC, as can a double-sided
 239 Si strip detector. The latter can also be mounted behind or inside the IC. All
 240 of the detectors are read out using a version of the MIDAS data acquisition
 241 system.

242 Both the PGAC and the IC are filled with isobutane as an ionization
 243 medium and have an active area of 154 mm by 54 mm, with a larger extent
 244 in the horizontal, dispersive direction than in the vertical direction. The
 245 PGAC, which measures 73 mm between entrance and exit foils, operates at
 246 pressures between 2 and 4 Torr while the 40 cm long, 16 anode segment IC
 247 is designed to operate at pressures of 10 – 100 Torr. Provisions have been
 248 made to mount up to 4 clover-shaped HPGe detectors of the type used in the
 249 GRIFFIN spectrometer [22] at the focal plane to study isomers and delayed
 250 activities.

251 The focal plane station has a set of 4 independently actuated 1.6 mm
 252 thick stainless steel plates just upstream of the PGAC that together consti-
 253 tute a slit system. Two of the plates are mounted on combined rotary and
 254 linear motion feedthroughs that present different profiles to the incident ions
 255 depending on their angle. In this way the focal plane slit system can obscure
 256 the entire focal plane except for 1 – 3 openings of continuously variable po-
 257 sition and width, enabling the simultaneous transmission of up to 3 charge

258 states.

259 5. Initial Measurements

260 Due to a flurry of last minute activity on the focal plane station vacuum
261 and control systems just prior to its first scheduled beam time, there was no
262 opportunity to first test the spectrometer with an alpha source. Hence initial
263 focussing and dispersion tests were carried out by bombarding a $4.5\text{ }\mu\text{m}$ thick
264 Au foil with an 80 MeV ^{36}Ar beam. The spectrometer was initially set to
265 transmit multiply scattered, 19 MeV $^{36}\text{Ar}^{13+}$ ions. The foil was sufficiently
266 thick that the multiply scattered Ar ions filled the angular and energy accep-
267 tances of the spectrometer. After observing a single, well-defined m/q peak
268 we set the fields for the same energy but charge state 13.5^+ and transmit-
269 ted the 13^+ and 14^+ charge states simultaneously. As shown in Figure 4,
270 the peaks of the two charge states were separated by the expected 66 mm
271 distance corresponding to the design m/q dispersion of 10 mm/%. The dif-
272 ferent peak heights reflect the charge state distribution of the transmitted
273 ^{36}Ar ions.

274 Following this initial in-beam test, we carried out a series of ion optical
275 studies with a ^{148}Gd α source to study the angular focussing, m/q disper-
276 sion, and energy dispersion cancellation. These tests will be described in a
277 forthcoming publication. The spectrometer was further tested when we bom-
278 barded a $900\text{ }\mu\text{g cm}^{-2}$ natural Cu target foil with both stable and radioactive
279 Na beams and set the spectrometer to detect fusion products. In these mea-
280 surements the $\pm 2^\circ$ horizontal aperture was in place, the PGAC was operated
281 at a pressure of 2 Torr, and the 3000 mm^2 Si detector was positioned directly

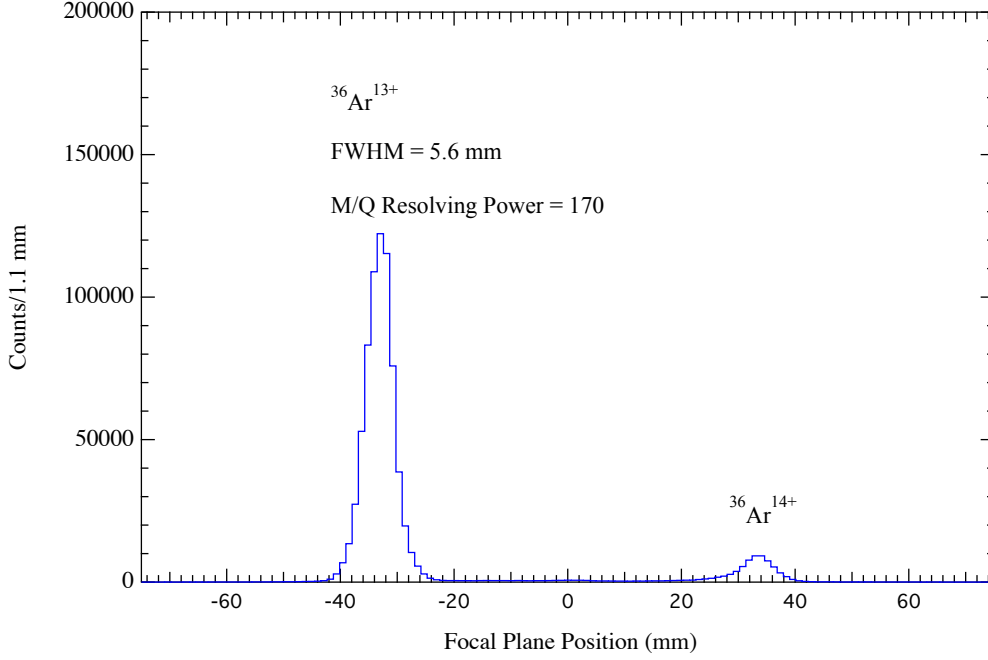


Figure 4: First m/q spectrum obtained with EMMA; it resulted from bombarding a 4.5 μm Au foil with an 80 MeV ^{36}Ar beam. Multiply-scattered Ar ions filled both the angular and energy acceptances of the spectrometer. The two detected charge states are separated by the 66 mm expected from the tuned m/q dispersion of 10 mm/%.

282 behind the PGAC to aid in distinguishing fusion products from scattered
 283 beam ions. We first bombarded the Cu target with an 84 MeV ^{23}Na beam
 284 from the ISAC offline ion source [23] and set the spectrometer for 18.4 MeV,
 285 81 u, 10^+ recoils.

286 After we obtained m/q spectra of the fusion products with several over-
 287 lapping spectrometer settings, the operations group delivered an 87 MeV,
 288 radioactive ^{24}Na beam produced in a SiC target by TRIUMF's 500 MeV
 289 proton beam and doubly ionized by a forced electron beam induced arc dis-
 290 charge ion source [24]. The operators succeeded in tuning more than 90%

291 of the radioactive beam through the 1 mm aperture of EMMA's Faraday
 292 cup. Beam intensities on target ranged from 1 to $4 \times 10^7 \text{ s}^{-1}$ and spectra
 293 were measured at several field settings. Figure 5 shows that obtained when
 294 the spectrometer was set for 17.1 MeV, 82 u, 10^+ recoils. Beam suppression
 295 at these settings exceeded a factor of 10^9 and the m/q resolving power was
 296 measured to be as large as 240 (FWHM), which is more than adequate to
 297 resolve masses around $A = 90$.

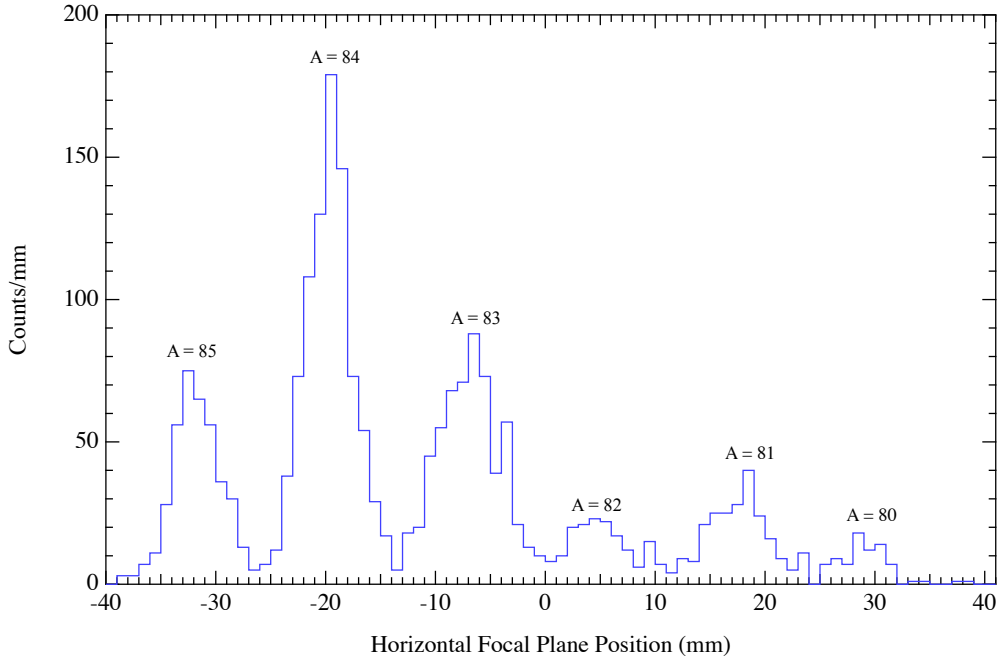


Figure 5: First m/q spectrum obtained using EMMA to detect products of reactions induced by a radioactive beam. A $900 \mu\text{g cm}^{-2}$ natural Cu foil was bombarded with an 87 MeV ^{24}Na beam and the spectrometer was tuned to transmit 17.1 MeV, 82 u, 10^+ recoils. This position spectrum from the PGAC was gated to include only events with an energy signal in the Si detector corresponding to fusion residues.

298 **6. Status and Future Plans**

299 High voltage conditioning is expected to be completed within the next 2
300 months, at which point the spectrometer will have been fully commissioned.
301 Four EMMA experiments and two letters of intent have been approved by
302 the TRIUMF subatomic physics experiment evaluation committee. All are
303 motivated by nuclear astrophysics and all but one of them require the in-
304 stallation of the TIGRESS γ -ray spectrometer around the EMMA target
305 position to provide spectroscopic information. This installation is planned
306 to be completed in the spring of 2019, at which point the EMMA scientific
307 program can begin in earnest.

308 **7. Acknowledgements**

309 BD acknowledges generous support from the Natural Sciences and Engi-
310 neering Research Council of Canada and is grateful to F. Cifarelli for his me-
311 chanical design work. OSK acknowledges support from the Villum Founda-
312 tion. TRIUMF receives federal funding via a contribution agreement through
313 the National Research Council of Canada. The UK authors acknowledge the
314 support of the Science and Technology Facilities Council.

- 315 [1] B. Davids, C. N. Davids, Nucl. Instrum. Methods Phys. Res. A 544
316 (2005) 565.
- 317 [2] R. E. Laxdal, M. Marchetto, Hyperfine Interactions 225 (2014) 79.
- 318 [3] G. Hackman, C. E. Svensson, Hyperfine Interactions 225 (2014) 241.
- 319 [4] C. A. Diget, S. P. Fox, et al., J. Instrum. 6 (2011) 2005P.

- 320 [5] T. M. Cormier, P. M. Stwertka, Nucl. Instrum. Methods Phys. Res. 184
321 (1981) 423.
- 322 [6] T. M. Cormier, P. M. Stwertka, Nucl. Instrum. Methods Phys. Res. 212
323 (1983) 185.
- 324 [7] P. Spolaore, J. D. Larson, et al., Nucl. Instrum. Methods Phys. Res. A
325 238 (1985) 381.
- 326 [8] C. Signorini, et al., Nucl. Instrum. Methods Phys. Res. A 339 (1994)
327 531.
- 328 [9] P. Spolaore, et al., Nucl. Instrum. Methods Phys. Res. A 359 (1995)
329 500.
- 330 [10] T. M. Cormier, et al., Nucl. Instrum. Methods Phys. Res. A 297 (1990)
331 199.
- 332 [11] J. D. Cole, et al., Nucl. Instrum. Methods Phys. Res. B 70 (1992) 343.
- 333 [12] C. J. Gross, et al., Nucl. Instrum. Methods Phys. Res. A 450 (2000) 12.
- 334 [13] A. K. Sinha, Nucl. Instrum. Methods Phys. Res. A 339 (1994) 543.
- 335 [14] S. Nath, Nucl. Instrum. Meth. Phys. Res. A 576 (2007) 403.
- 336 [15] H. Ikezoe, et al., Nucl. Instrum. Methods Phys. Res. A 376 (1996) 420.
- 337 [16] H. Ikezoe, et al., Nucl. Instrum. Methods Phys. Res. B 126 (1997) 340.
- 338 [17] T. Kuzumaki, H. Ikezoe, et al., Nucl. Instrum. Methods Phys. Res. A
339 437 (1999) 107.

- 340 [18] C. N. Davids, J. D. Larson, Nucl. Instrum. Methods Phys. Res. B 40
341 (1989) 1224.
- 342 [19] C. N. Davids, et al., Nucl. Instrum. Methods Phys. Res. B 70 (1992)
343 358.
- 344 [20] B. B. Back, et al., Nucl. Instrum. Methods Phys. Res. A 379 (1996) 206.
- 345 [21] H. Wollnik, J. Brezina, M. Berz, Nucl. Instrum. Methods Phys. Res.
346 A258 (1987) 408.
- 347 [22] A. B. Garnsworthy, C. E. Svensson, M. Bowry, R. Dunlop, A. D.
348 MacLean, B. Olaizola, J. K. Smith, et al., Nucl. Instrum. Meth. Phys.
349 Res. A 918 (2019) 9.
- 350 [23] K. Jayamanna, Hyperfine Interactions 225 (2014) 51.
- 351 [24] P. G. Bricault, F. Ames, M. Dombsky, P. Kunz, J. Lassen, Hyperfine
352 Interactions 225 (2014) 25.